Supplement of Atmos. Chem. Phys., 26, 9061–9082, 2026
https://doi.org/10.5194/acp-26-9061-2026-supplement


Atmospheric Chemistry and Physics
Open Access
EGU

*Supplement of*

# Assessing raindrop evaporation over northern Western Ghats from stable isotope signature of rain and vapour

**Sheena Sunil Nimya et al.**

*Correspondence to:* Saikat Sengupta (saikat@tropmet.res.in)

*Supplement of*

# Assessing raindrop evaporation over northern Western Ghats from stable isotope signature of rain and vapour

Sheena Sunil Nimya [1,2], Sundara Pandian Rajaveni[1], Saikat Sengupta[1*], Sourendra Kumar Bhattacharya[3], Nandhini Ananthvel[1]

[1]Center for Climate Change Research, Indian Institute of Tropical Meteorology, Ministry of Earth Sciences, Pune-411008, India

[2]Department of Earth, Atmospheric and Planetary Sciences, Purdue University, West Lafayette, IN, USA

[3]Institute of Earth Sciences, Academia Sinica, Taipei 11529, Taiwan

*Correspondence: Saikat Sengupta (saikat@tropmet.res.in)

**Introduction**

The supplementary Information contains materials related to sample collection methods, isotope analysis, back trajectory analysis, isotope correlation with meteorological parameters, Bootstrap method of slope determination in the Δδ-Δd plot, cloud liquid water content, drop introduction height and cloud base determination, derivation of RH, T and vapour isotope profiles from Radiosonde and TES for the BCIM, and sensitivity analysis of the model predictions.

**S1 Rain sample collection procedure**

Rain samples were collected over a 24-hour interval (8:30 am to 8.30 am the next day, Indian Standard Time) using a sampling device made in accordance with the International Atomic Energy Agency guidelines. A schematic of the setup is shown in Fig. S1. Samples were collected on all rainy days with a rain rate≥0.1 mm day$^{-1}$. A 10-Liter carboy bottle, fitted with a 25 cm-diameter funnel, was mounted ~1 m above ground level to avoid contributions from ground splashing. A tube attached to the funnel tip reached the bottom of the bottle, reducing the exposed surface area and minimizing evaporation. After collection, the samples were transferred to 8-ml polycarbonate bottles and stored in a dark, cold place. The date and time of collection are labeled on the sample bottle. The sampling and storage procedures were carefully selected to minimize sample evaporation (Rajaveni et al., 2024). A total of 59 rain samples were collected. The samples were analyzed as soon as possible after collection at the Indian Institute of Tropical Meteorology (IITM), Pune.

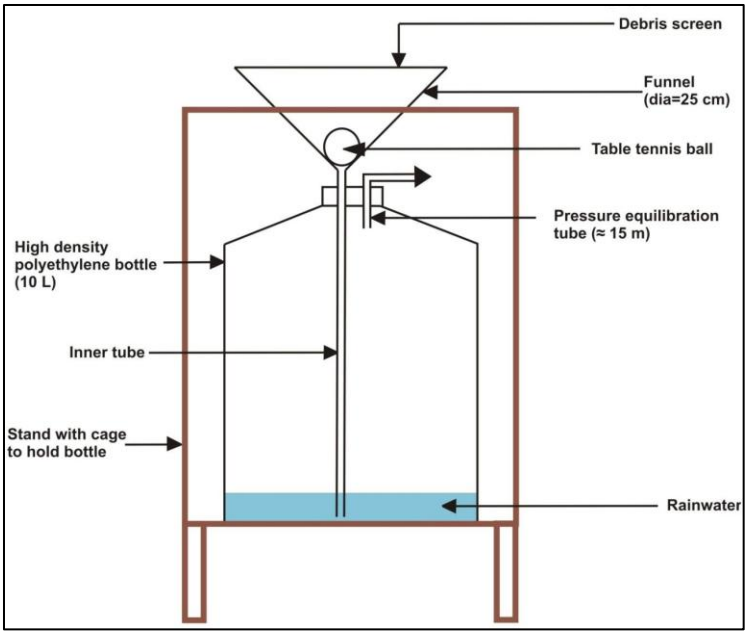


**Figure S1.** Schematic picture of the device for rain sample collection

**S2 Vapour sample collection Procedure**

An in-house fabricated glass system (Fig. S2) was used for vapour sample collection. The ambient air was pulled through a PTFE tube by a diaphragm pump at a flow rate of ~800 ml $min^{-1}$ (to ensure laminar flow in the collection line) and then passed through a glass condenser (Trap-1) immersed in a cold alcohol slurry in a Dewar flask. The slurry temperature was maintained at -80 °°X using liquid nitrogen. At this temperature, atmospheric moisture condenses into ice, leaving other gases to be pumped out. The airflow was controlled by a Cole-Parmer flow meter (model MR3A138VVTCP). To obtain adequate condensed moisture, sampling was carried out for 3 to 4 hours, the exact period depending on the ambient specific humidity. One sample was collected per day, usually between 9.30 am and 2 pm. The sampling period was usually adequate for the amount of condensed vapour to be at least double the amount required for isotope analysis (i.e., about 1ml). We added a second trap (Trap-2) to assess the collection efficiency. A complete collection by Trap-1 is ensured when there is no ice in Trap-2. After sampling, the condensers were brought to room temperature to convert the ice sample to water. The water samples were then pipetted into 2 ml glass vials and stored. During our study period of nearly 4 months (July to October 2019), a total of 46 vapour samples were collected, and among them, 29 sample collection dates coincided with simultaneous rain sample collection dates.

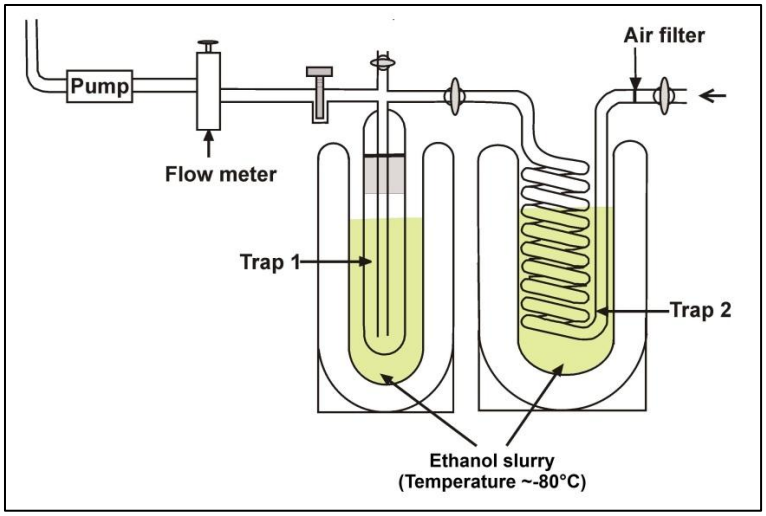


**Figure S2.** Schematic picture of the device for vapour sample collection

We examined the collection efficiency in two ways: (1) we checked that no condensate exists in Trap-2 and (2) we calculated the amount of vapour expected to be condensed in Trap-1 using ambient specific humidity and flow rate and compared the derived value with the water collected in Trap-1. Table S1 shows these calculations. The mean condensation efficiency was 109±15 % indicating an efficient collection of the water vapour in Trap-1 without loss.

**Table S1.** Fraction of water vapour condensed during vapour sampling on different days, calculated using a flow rate of 800 ml $min^{-1}$ and an air density of 1.18 kg $m^{-3}$

| Date (dd-mm) | Volume of water vapour condensed (ml) | Sampling period (hr) | Relative humidity (%) | Air temperature (°C) | Saturation vapour pressure at air temperature, $e_s$ (hPa) | Actual vapour pressure, e (hPa) | Mixing ratio (w) | Specific humidity (q) g/kg | Volume of air drawn (ml) | Mass of air drawn (g) | Mass of vapour collected (g) | Mass of vapour condensed (g) | Fraction of vapour condensed (%)* |
|---|---|---|---|---|---|---|---|---|---|---|---|---|---|
| 22-07 | 4 | 3.5 | 65 | 30.2 | 42.9 | 27.9 | 0.019 | 18.5 | 144000 | 168 | 3.1 | 4.0 | 129 |
| 24-07 | 6 | 3.5 | 80 | 26.6 | 34.8 | 27.9 | 0.019 | 18.4 | 168000 | 198 | 3.7 | 6.0 | 164 |
| 25-07 | 4 | 3.5 | 84 | 25.9 | 33.4 | 28.1 | 0.019 | 18.6 | 168000 | 198 | 3.7 | 4.0 | 108 |
| 26-07 | 3.5 | 3 | 93 | 25.5 | 32.7 | 30.4 | 0.021 | 20.1 | 144000 | 199 | 3.4 | 3.5 | 102 |
| 30-07 | 4 | 3.5 | 91 | 25.6 | 32.8 | 29.9 | 0.020 | 19.8 | 168000 | 199 | 3.9 | 4.0 | 102 |
| 31-07 | 4 | 3.5 | 85 | 26.0 | 33.6 | 28.6 | 0.019 | 18.9 | 168000 | 198 | 3.8 | 4.0 | 106 |
| 01-08 | 3.5 | 3 | 89 | 26.2 | 34.0 | 30.2 | 0.020 | 20.0 | 144000 | 170 | 3.4 | 3.5 | 103 |
| 02-08 | 4.5 | 3.5 | 92 | 26.2 | 33.9 | 31.2 | 0.021 | 20.7 | 168000 | 198 | 4.1 | 4.5 | 110 |
| 05-08 | 4.5 | 3.5 | 97 | 27.0 | 35.6 | 34.5 | 0.023 | 22.9 | 168000 | 198 | 4.5 | 4.5 | 99 |
| 06-08 | 4 | 3.5 | 90 | 26.7 | 34.9 | 31.5 | 0.021 | 20.9 | 168000 | 198 | 4.1 | 4.0 | 97 |
| 07-08 | 4 | 3.5 | 86 | 26.1 | 33.9 | 29.2 | 0.020 | 19.3 | 168000 | 198 | 3.8 | 4.0 | 104 |
| 08-08 | 3.5 | 3 | 84 | 26.7 | 35.1 | 29.5 | 0.020 | 19.5 | 144000 | 170 | 3.3 | 3.5 | 106 |
| 09-08 | 5 | 3.5 | 85 | 26.5 | 34.6 | 29.4 | 0.020 | 19.5 | 168000 | 198 | 3.9 | 5.0 | 130 |
| 13-08 | 3.5 | 3 | 84 | 27.6 | 36.9 | 31.0 | 0.021 | 20.5 | 144000 | 169 | 3.5 | 3.5 | 101 |

| | | | | | | | | | | | | | |
|---|---|---|---|---|---|---|---|---|---|---|---|---|---|
| 14-08 | 4.8 | 3.5 | 81 | 27.3 | 36.2 | 29.3 | 0.020 | 19.4 | 168000 | 198 | 3.8 | 4.8 | 125 |
| 21-08 | 4 | 3.5 | 74 | 26.9 | 35.4 | 26.2 | 0.018 | 17.3 | 168000 | 198 | 3.4 | 4.0 | 117 |
| 22-08 | 4.5 | 3.5 | 79 | 27.5 | 36.8 | 29.1 | 0.020 | 19.3 | 168000 | 197 | 3.8 | 4.5 | 118 |
| 23-08 | 3.5 | 3.5 | 71 | 27.0 | 35.7 | 25.3 | 0.017 | 16.7 | 168000 | 198 | 3.3 | 3.5 | 106 |
| 27-08 | 3.5 | 3 | 78 | 27.2 | 36.1 | 28.2 | 0.019 | 18.7 | 144000 | 169 | 3.2 | 3.5 | 111 |
| 30-08 | 4 | 3.5 | 78 | 26.5 | 34.6 | 27.0 | 0.018 | 17.9 | 168000 | 198 | 3.5 | 4.0 | 113 |
| 03-09 | 3.5 | 3 | 84 | 25.9 | 33.4 | 28.0 | 0.019 | 18.6 | 144000 | 170 | 3.2 | 3.5 | 111 |
| 04-09 | 4 | 3.5 | 88 | 26.1 | 33.8 | 29.7 | 0.020 | 19.7 | 168000 | 198 | 3.9 | 4.0 | 102 |
| 05-09 | 3.5 | 3 | 84 | 26.7 | 35.1 | 29.5 | 0.020 | 19.5 | 144000 | 170 | 3.3 | 3.5 | 106 |
| 06-09 | 4 | 3.5 | 87 | 26.3 | 34.3 | 29.8 | 0.020 | 19.7 | 168000 | 198 | 3.9 | 4.0 | 102 |
| 09-09 | 3.5 | 3 | 93 | 26.5 | 34.7 | 32.2 | 0.022 | 21.4 | 144000 | 170 | 3.6 | 3.5 | 96 |
| 16-09 | 3.5 | 3 | 84 | 26.7 | 35.1 | 29.5 | 0.020 | 19.5 | 144000 | 170 | 3.3 | 3.5 | 106 |
| 18-09 | 4 | 3 | 97 | 27.2 | 36.2 | 35.1 | 0.024 | 23.3 | 144000 | 169 | 3.9 | 4.0 | 101 |
| 19-09 | 4.5 | 3.5 | 86 | 26.7 | 35.1 | 30.2 | 0.020 | 20.0 | 168000 | 198 | 4.0 | 4.5 | 114 |
| 25-09 | 3.4 | 3 | 81 | 29.4 | 41.1 | 33.3 | 0.023 | 22.1 | 144000 | 168 | 3.7 | 3.4 | 91 |
| *Mean fraction of vapour condensed 109(±15) % | | | | | | | | | | | | | |

**S3 Isotope analysis**

All rainwater samples are measured using a laser-based liquid water isotope analyzer (LWIA; Model No. TIWA-45-EP), manufactured by Los Gatos Research (LGR), with routine analytical precision of 0.1‰ and 1‰ for δ18O and δD, respectively, determined using five laboratory standards. These standards are periodically calibrated with respect to IAEA primary standards. The measurement procedure followed a standard protocol described below. As mentioned above, 29 sampling days were common for both vapour and rain samples. These samples are especially important for the present study.

The LWIA simultaneously measures $\delta^{18}O$ and δD of liquid samples, with each measurement taking ~1.5 minutes. 1 mL aliquots of water samples (both rain and standards) are transferred into 2 mL glass vials capped with pre-sealed silicone septa and placed sequentially in an auto-sampler block. During measurement, 1.2 µL of liquid is sampled by the auto-sampler from the vial and injected into an injector block (preheated at ~70° C). Water vapour produced in the injector block is then transferred to the isotope analyzer through a Teflon tube. Between two consecutive injections, dry air is passed through the cavity, and the entire cavity is pumped to eliminate sample memory from previous measurements. In high-throughput mode, each sample is measured 9 times via 9 separate injections, with the first 4 injections discarded to eliminate memory effects. The data measured by the analyzer are then calibrated to Vienna Standard Mean Ocean Water (VSMOW) using post-processing software.

**S4 Back Trajectory analysis**

To identify the moisture sources of the vapor and rain reaching our study area, a 48-hour air-mass back-trajectory analysis was conducted at the 850 mb pressure level using the NOAA Hybrid Single-Particle Lagrangian Integrated Trajectory (HYSPLIT) model (Draxler and Hess, 1997). The model tracks the backward movement of air parcels from a given location over a desired period. The Global Data Assimilation System (GDAS; 1°×1°; Kanamitsu, 1989) dataset is used for this calculation. The trajectories shown in Fig. S3 indicate that moisture is mostly from the

Arabian Sea, carried inland by wind systems that impinge almost perpendicularly on the coast at Bombay and reach Pune 150 km downstream in a matter of hours (speed 20-40 km h-1).

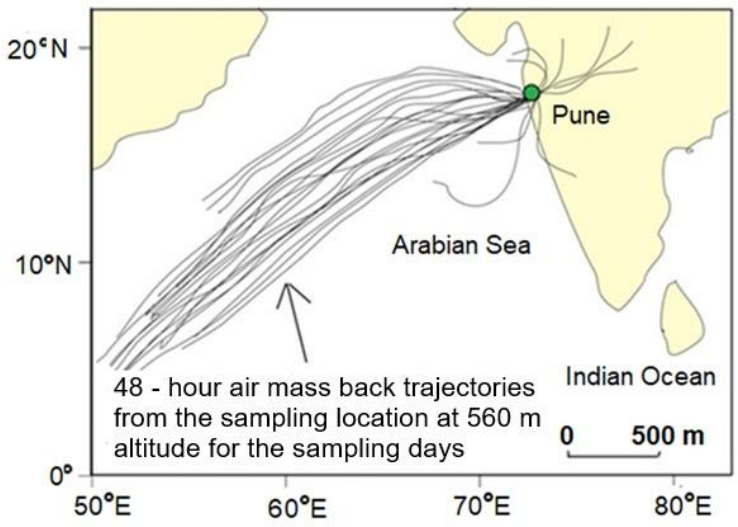


**Figure S3.** 48-hour air mass back trajectories calculated using the HYSPLIT model for Pune (located at an altitude of 560 m) for the sampling dates during the monsoon of 2019. Each black line represents the trajectory for one sampling day at 850 mb pressure level.

**S5 Cloud Liquid Water Content peak, drop introduction height and Cloud Base**

We used the isotope model BCIM for the 29 days when both rain and vapour samples were collected. To run the BCIM for a given day, a drop introduction altitude for that day is required as input. This is not known a priori. A profile of Cloud Liquid Water Content (CLWC) provides vertical variation of liquid water content within the cloud. The altitude at which CLWC is maximum corresponds to the height where the likelihood of raindrop formation is highest. The daily average vertical profile of CLWC (mg $m^{-3}$) during the study period was obtained from the ERA5 dataset for the 29 selected days and is plotted in Fig. S4. The height at which the CLWC is maximum is considered as the drop introduction height for Run-2 and Run-3 of the BCIM simulations, and their values are tabulated in Table S2. The mean peak value for the 29 selected dates is about 850 mb. For the Rayleigh case (Run-1), we set the 850 mb level as the drop introduction height for all dates. We note that in Run-1 (corresponding to the Rayleigh condensation model), the first attainment of the RH=100% level occurred at an altitude below 850 mb and can be taken as the cloud base.

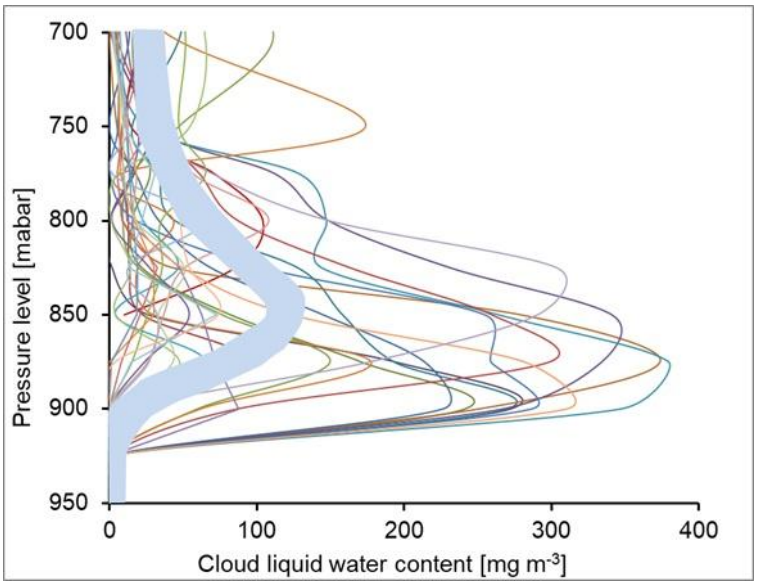


**Figure S4.** Cloud liquid water content (CLWC; mg $m^{-3}$) variation with altitude over Pune for the 29 sampling dates when both vapour and rain samples were collected and analyzed. Each coloured line shows the daily average CLWC from the ERA5 dataset. The thick, bluish-grey band shows the mean CLWC profile for the entire study period.

As mentioned in the main text, the Lifting Condensation Level (LCL) is taken as the cloud base. The RH and T profiles from the radiosonde data at various heights (with extrapolated ground-level values; see SI-6b) are used to estimate the LCL using the Skew-T-Log P diagram for the 29 selected days. The LCL varies from 820 mb to 900 mb, and the average height is 890 ± 20 mb (about 1050 m; see Table S2). We notice that the LCL is always below (about 600 m on average) the corresponding day's CLWC peak, as it should be. Therefore, the drop falls partly through a zone of 100% RH corresponding to the distance between the LCL to the CLWC peak. There are six extreme cases in which the LCL-CLWC peak distance exceeds 100 m, and nine cases in which the distance is close to zero. Table S2 shows the LCL values and the altitude of CLWC peaks for the 29 days. Interestingly, our data show an intriguing phenomenon: radiosonde RH does not reach 100% at the LCL. However, this fact is well known (Song et al., 2020) and arises from a key distinction between LCL calculations and the radiosonde RH profile. The RH at the LCL refers to the parcel's humidity, which does not necessarily represent the surrounding environmental humidity measured by the radiosonde sensor at that pressure level. The LCL is found on a skew-T diagram by taking the parcel's initial temperature and following a dry adiabatic upward, while simultaneously following the saturation mixing ratio line (starting from the parcel's initial dewpoint) upward. The intersection of these two lines is the LCL.

The pertinent question for BCIM application is which RH value should be considered in the zone between the drop-formation height and LCL. Guided by the reference RH profile presented by Graf et al. (2019) for the Rayleigh model, we assume that RH remains 100% between the LCL and the drop introduction height (CLWC peak). Below the LCL, we assume that the RH values as obtained from the radiosonde data pertain. However, because the radiosonde RH does not smoothly approach 100% at the LCL, the adopted profile shows a small jump at that level. This is an artifact because we force the radiosonde RH profile to jump to 100% at the LCL. In effect, we are using a

hybrid RH profile with two inputs: observed Radiosonde values below the LCL and the model requirement of 100% RH at and above the LCL.

**Table S2**. Lifting Condensation level (LCL) and the level (in mbar) at which CLWC is maximum for 29 sampling days. The LCLs are estimated from the radiosonde analysis, and the CLWC peak data are obtained from the ERA5 gridded dataset.

| No. of Days | Date | CLWC Peak level (mbar) | LCL (mbar) |
|---|---|---|---|
| 1 | 22-07-2019 | 800 | 823 |
| 2 | 24-07-2019 | 880 | 884 |
| 3 | 25-07-2019 | 900 | 900 |
| 4 | 26-07-2019 | 900 | 900 |
| 5 | 30-07-2019 | 875 | 900 |
| 6 | 31-07-2019 | 880 | 899 |
| 7 | 01-08-2019 | 875 | 884 |
| 8 | 02-08-2019 | 875 | 900 |
| 9 | 05-08-2019 | 850 | 900 |
| 10 | 06-08-2019 | 875 | 900 |
| 11 | 07-08-2019 | 875 | 878 |
| 12 | 08-08-2019 | 880 | 882 |
| 13 | 09-08-2019 | 875 | 889 |
| 14 | 13-08-2019 | 775 | 877 |
| 15 | 14-08-2019 | 850 | 879 |
| 16 | 21-08-2019 | 875 | 879 |
| 17 | 22-08-2019 | 850 | 900 |
| 18 | 23-08-2019 | 720 | 863 |
| 19 | 27-08-2019 | 700 | 882 |
| 20 | 30-08-2019 | 700 | 900 |
| 21 | 03-09-2019 | 894 | 897 |
| 22 | 04-09-2019 | 900 | 900 |
| 23 | 05-09-2019 | 700 | 876 |
| 24 | 06-09-2019 | 850 | 880 |
| 25 | 09-09-2019 | 700 | 898 |
| 26 | 16-09-2019 | 800 | 882 |
| 27 | 18-09-2019 | 825 | 900 |
| 28 | 19-09-2019 | 825 | 900 |
| 29 | 25-09-2019 | 850 | 880 |

In this context, we show (Fig. S5) the altitude variation of the three related parameters: the 100% RH level in Run-1 (Rayleigh model), LCL in Run-2 and Run-3, and CLWC peak in Run-2 and Run-3. As discussed in the main text, the LCL and CLWC peaks are considered the cloud base and drop introduction height in Run-2 and Run-3, but in Run-1, the first attainment of RH=100% is considered the cloud base. RH=100% level values in Run-1 are seen to be lower than the LCL values (on average by about 500 meters). It is known that cloud base height values (RH=100% level) based on lapse rates are usually lower estimates. Lapse rates mostly predict low clouds, which are not seen in Pune (Ernest Raj et al., 1996). Similarly, a recent study by Craven et al. (2002) from the central United States found that LCL estimates based on surface temperature and RH, known as the surface-based parcels LCL (SBLCL) method, are consistently lower than observed cloud bases.

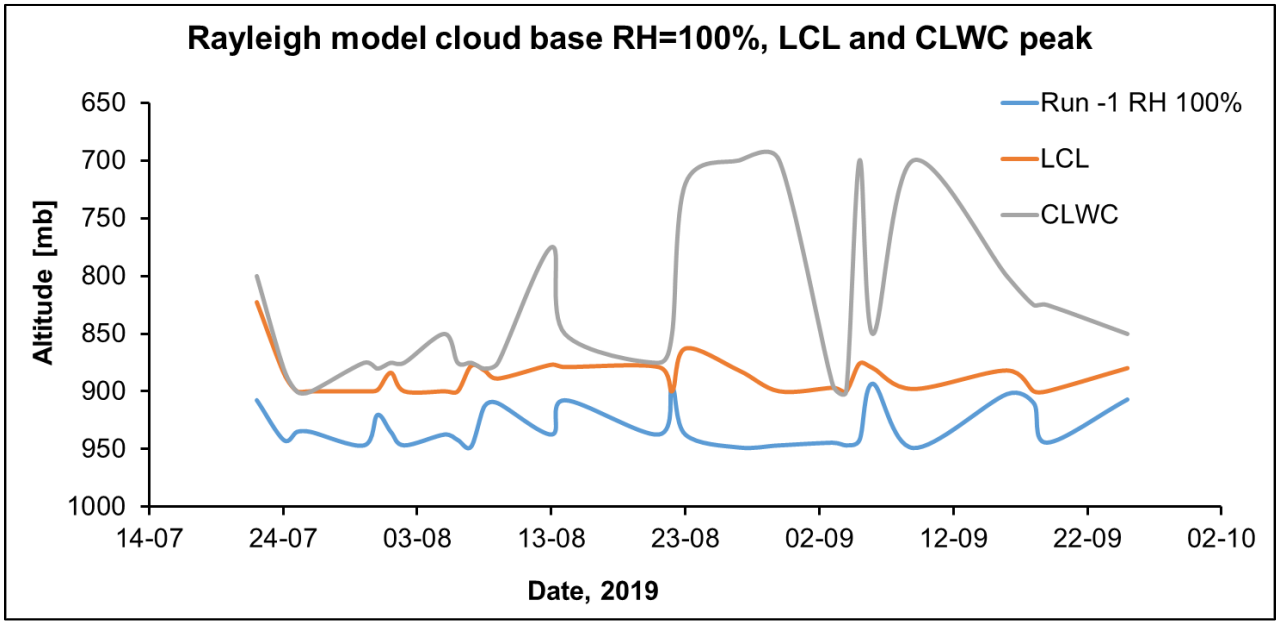


**Figure S5.** The altitude variations of the Rayleigh model (Run-1) RH=100% level (cloud base), LCL and CLWC peak for Run-2 and Run-3 on different dates are shown in three colours: Blue, Orange, and Grey, respectively.

**S6 Input profiles for BCIM**

**S6.1 Construction of vapour isotope profiles from TES for Run-2**

The BCIM requires four input profiles: relative humidity (RH), temperature (T), vapour δD ($\delta D_v$), and d-excess ($d_v$) for each run. Below, we explain in detail how we constructed the $\delta D_v$ and $d_v$ profiles for each date.

1: We analyzed available TES $\delta D_v$ profiles (digital values) for the years 2005-2007 and adopted three profiles which correspond to the Minimum, Mean and Maximum surface vapour isotope values. These values were -125.2‰ ($v_1$), -80.8‰ ($v_2$) and –63.0‰ ($v_3$).

2. These three profiles were fitted with equations of the type: $Ah_3+Bh_2+Ch+ D$, where h is the altitude, giving us three values for each coefficient, i.e., for each of the A, B, C and D coefficients, corresponding to three surface $\delta D_v$ values ($v_1$, $v_2$, $v_3$) given above. For example, $A_1$, $A_2$ and $A_3$ for $v_1$, $v_2$ and $v_3$.

3. We now need to find the coefficient sets for each day where the surface values are different from $v_1$, $v_2$ and $v_3$. This was done by fitting each coefficient as a function of the surface value (v) using data from 2 (above). Once we got the fitting equation ($av_2+bv+c$) for each coefficient (A or B or C or D) as a function of the surface value v, we can get the coefficient for each day corresponding to the surface value (v) observed for that day (Fig. S6a)

This exercise was necessary to translate the digital TES values into an analytical form, allowing for the easy calculation of vapour isotope values at each height (at one meter resolution required for the BCIM run) from the uppermost drop introduction point to the ground level, resulting in a smooth-shaped profile.

A similar exercise was conducted to obtain the daily d-excess profile from the LMDZ GCM output for Pune in 2019 after normalising the data to the surface-measured vapour d-excess value. LMDZ is a global circulation model in which the dynamical equations are discretized on a latitude-longitude grid, with a standard resolution of 2.5° × 3.75° and 19 vertical levels. Water in its vapour and condensed form is advected by the Van Leer advection scheme (Van Leer, 1977), which is a monotonic second-order finite volume scheme. The physical package (Hourdin et al., 2006) includes the Emanuel convective parameterization (Emanuel, 1991; Grandpeix et al., 2004) coupled to the Bony and Emanuel (2001) cloud scheme. Wind (u, v) fields are nudged by ECMWF. Water isotopic species ($H_2{}^{16}O$, $H_2{}^{18}O$ and HDO) are transported and mixed passively by the large-scale advection and various air mass fluxes. In brief, the d-excess profiles of vapour ($d_v$) were calculated using the available $\delta D_v$ and $\delta^{18}O_v$ profiles from the LMDZ outputs for three cases (Mean, Max and Min surface values), fitting the appropriate polynomials and then constructing the d-excess profiles from these values for three cases with five coefficients. Again, fitting was performed for each polynomial coefficient (A, B, C, D, and E) as a function of surface value, and the resulting coefficients were used to obtain the d-excess profile for each day.

This means that by using the observed ground vapour value as a boundary constraint, we obtain the desired profiles for $\delta D_v$ and $d\text{-excess}_v$ from an analytical fitting of data from TES (adopted) and LMDZ. We used a multi-order polynomial to achieve the best possible fit, especially for d-excess, because when estimating uncertainty, we can account for uncertainties in the TES and LMDZ without worrying about the fitting uncertainties. We illustrate the technique for a three-parameter case for $\delta D_v$ profile (initially used for Pune). The fit (Figure S6a) has three coefficients, A, B, and C (note that we later use four coefficients).

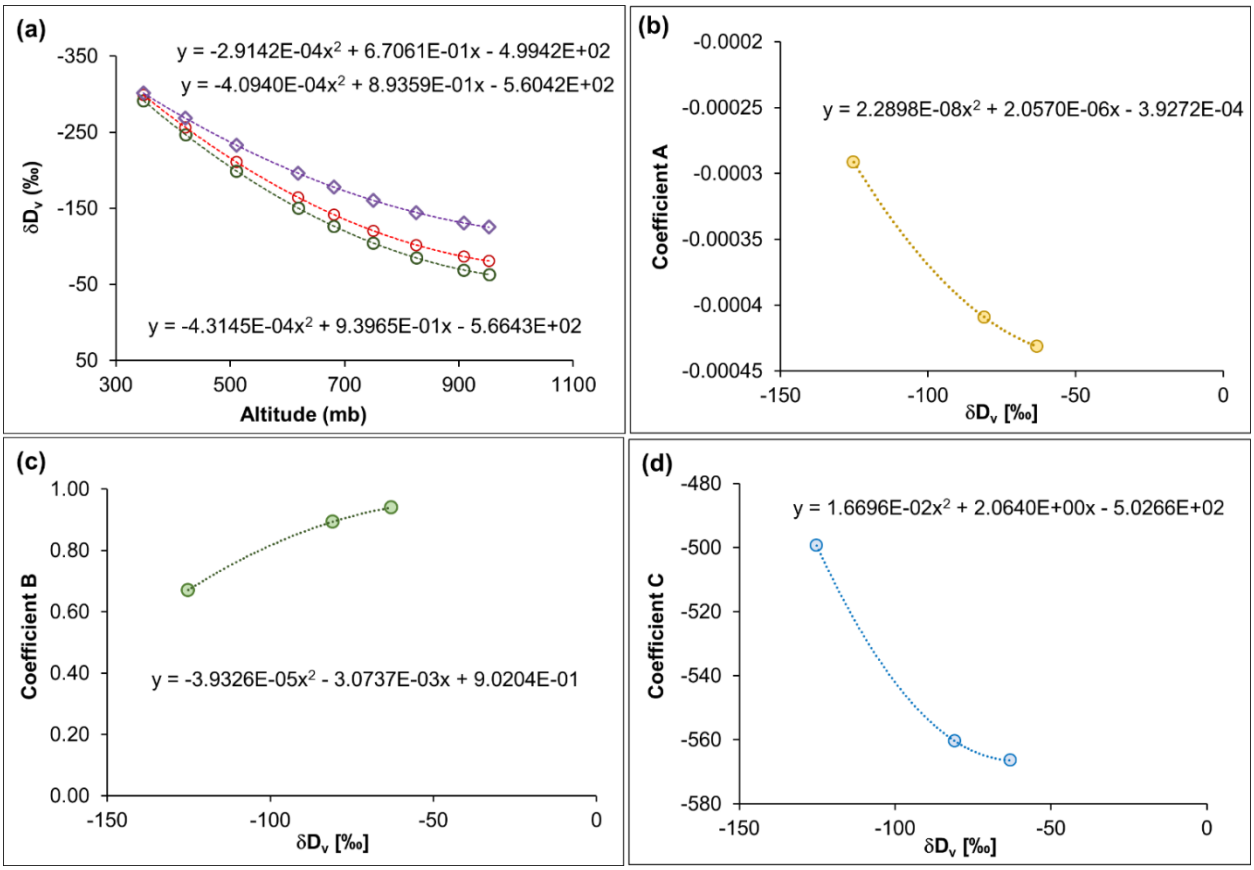


**Figure S6.** Demonstrating the construction of TES isotope profiles for a three-parameter case: **(a)** vapour $\delta D_v$ profile as a function of altitude (mbar). Three profiles were constructed from the mean, maximum, and minimum surface values available in the TES data set. Three second-order polynomial fits ($y = Ax^2 + Bx + C$) used to fit the data as a function of altitude (for each case) are also shown in the figure. The coefficients A, B and C as a function of surface $\delta D_v$ values are plotted in **(b), (c) and (d),** respectively, and best-fit equations are derived. These equations can now be used to derive the three- parameter coefficient set for any given date using the measured surface value for that date.

We note that the three TES profiles are nearly parallel and change only a little within 950 to 850 mbar, which was the relevant interval for the below-cloud zone over Pune. If we take the day-to-day changes in the CLWC peak, which is considered the drop introduction height, we need to go up in these profiles to get the $\delta D_v$. A, B and C are the surface value dependent coefficients and they are fitted with surface values as variables (shown in Fig. S6). Once we have the coefficient set for a particular date, we can use the fitted polynomials to calculate $\delta D_v$ as a function of height for that day.

**S6.2 Constructed input profiles for Run-1, Run-2 and Run-3 in the BCIM**

The two figures (Fig. S7 and S8) show the input profiles of meteorological and isotope parameters, respectively. The same RH and T profiles are used for both Run-2 and Run-3. We note that the first radiosonde data is collected not exactly at ground level but at about 50-60 meters above the ground by a different instrument (a thin-film capacitive polymer sensor). This makes a slight difference between the interpolated RH surface values from radiosonde and surface observations on the same day. Therefore, a slight difference exists between Run-1 and Run-2. The difference is not large, usually within a few percent, except for three days, when it varies from 11% to 15%. We also see that

the RH profiles in Run-2 differ significantly from those in Run-1. This is because the Run-1 profile is obtained from a calculation using a constant lapse rate, whereas the Run-2 profile is based on radiosonde measurements as a function of height.

The input profiles of $\delta D_v$ and $d_v$ for various days (see Fig. S8) in Run-1 (a and b), Run-2 (c and d) and Run-3 (e and f) show that the $\delta D_v$ values decrease greatly with altitude (about 20 to 30 ‰ from surface to 700 mb altitude). In contrast, the $d_v$ values remain reasonably constant with height in each case. The Run-3 values are about 6 ‰ lower on average than the values for Run-1 and Run-2. These lower $d_v$ values provide a better fit in Run-3 as discussed in the main text.

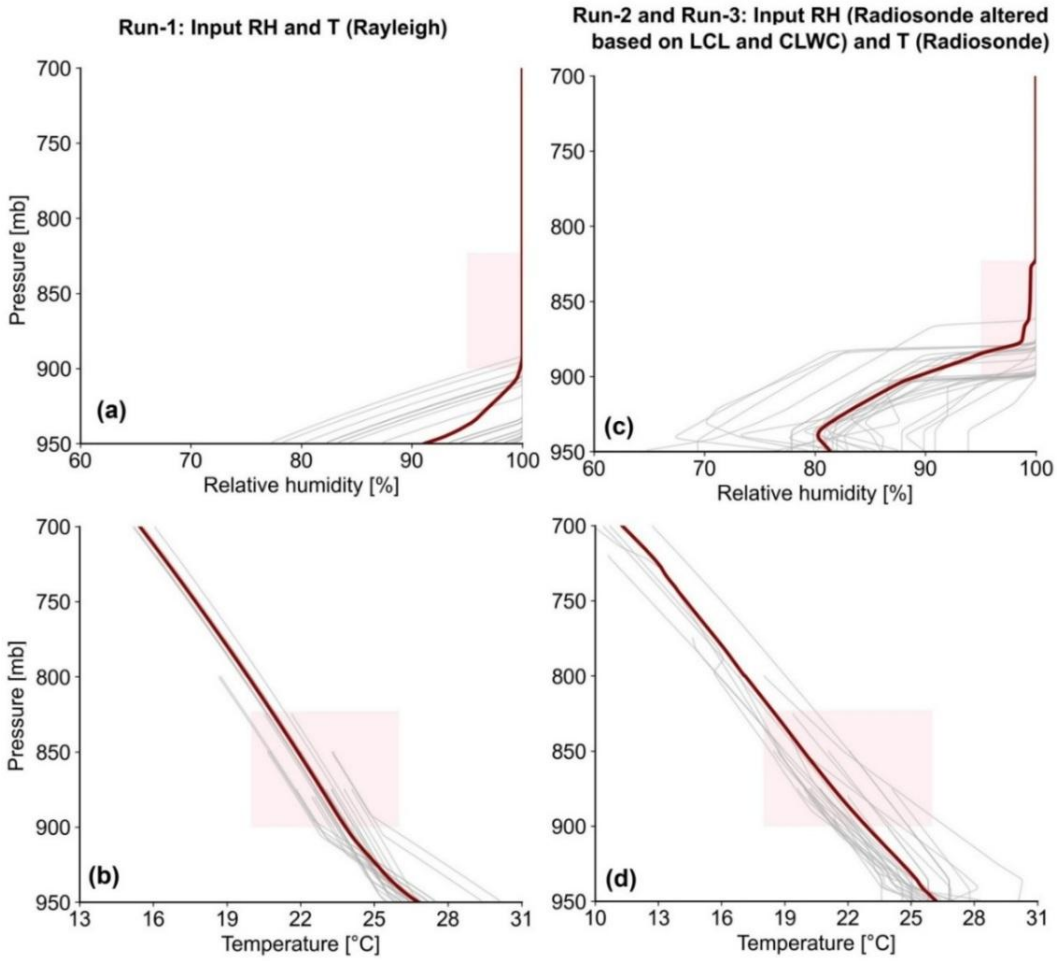


**Figure S7.** Input RH (**a and c**) and Temperature (**b and d**) profiles of the atmosphere for various runs used in the BCIM. The bold maroon line indicates the average profile. Details of the runs are discussed in section 3.2. in the main text; the run numbers are given above (in bold letters).

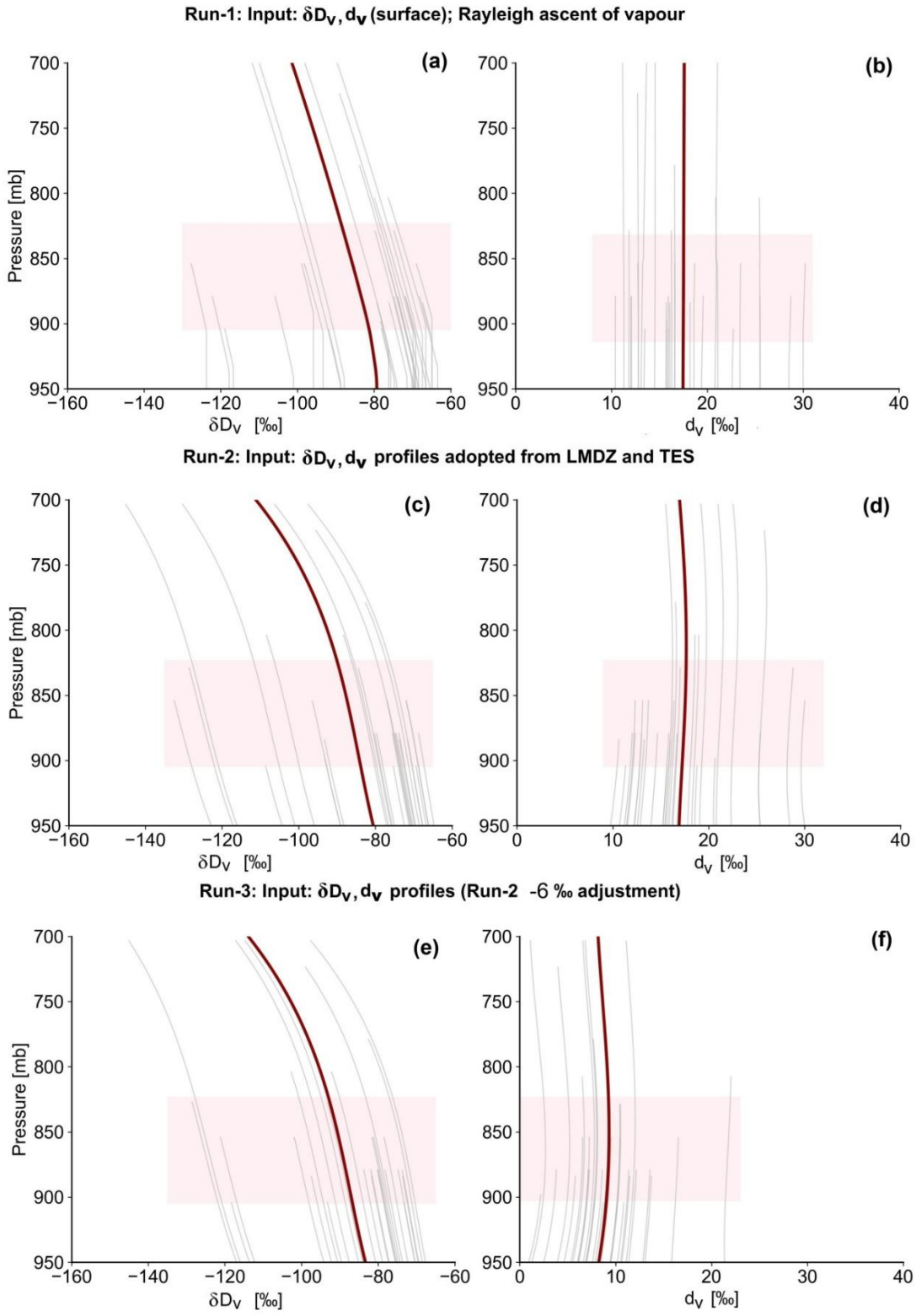


**Figure S8.** Input profiles of $\delta D_v$ and $d_v$ for various days in Run-1 (**a and b),** Run-2 (**c and d), and Run-3** (**e and f**). The bold maroon line indicates the average profiles.

**S7 How well the air is mixed below the cloud base**

In the BCIM, the $\delta D_v$ values in the Rayleigh assumption do not change in the sub-cloud layer, i.e., below the level where RH attains the value of 100% by considering the lapse rate. In this assumption, the specific humidity remains constant below the cloud base, and the increase in RH occurs solely due to a decrease in the ambient temperature. This raises the question of whether we can assume a well-mixed condition in the sub-cloud region. The ERA5 data indicate that this condition is invalid. We note that this is taken into account when we construct $\delta D$ profiles for Run-2 and Run-3. For these runs, a notable depletion of $\delta D_v$ (~20 ‰) at high altitude (~700 mb) is observed (Fig. S8b), corresponding to a decrease in specific humidity (between the surface and drop introduction altitude). A study by Noone (2012) showed that, in reality, the relationship between specific humidity (q) and $\delta D_v$ does not always follow the Rayleigh distillation pattern (Fig. S9a). Although our input $\delta D_v$ profiles are not based on the q profiles, q, as derived from the radiosonde data, shows an upward decreasing trend (Fig. S9b), suggesting that the sub-cloud layer is not well mixed. This is further supported by the radiosonde temperature data, which also decrease with altitude (Fig. S7d).

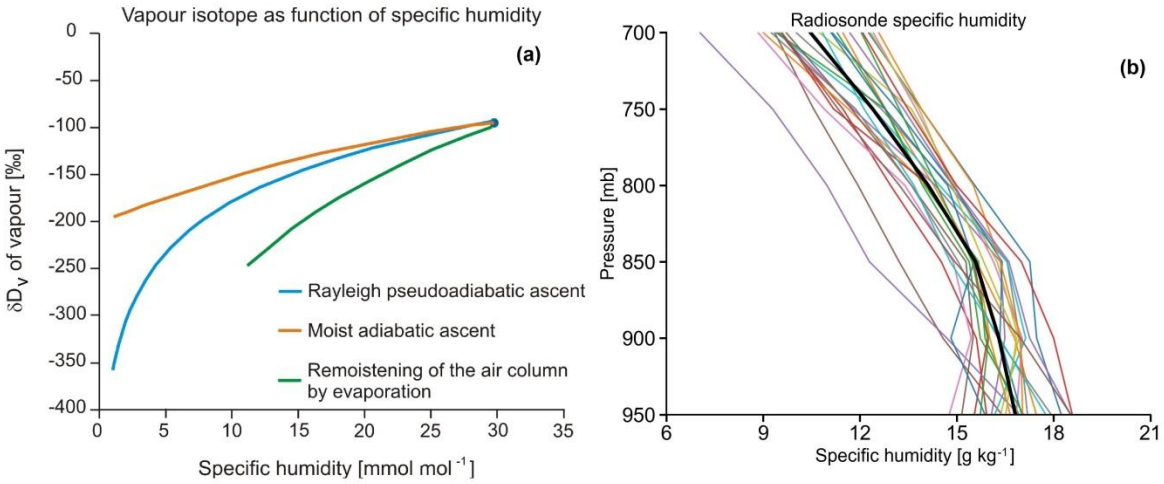


**Figure S9 (a)** Theoretical predictions of the changes in $\delta D_v$ as a function of specific humidity. The Rayleigh curve (blue) represents a pseudo-adiabatic ascent of air mass with initial specific humidity of 30 mmol $mol^{-1}$ and $\delta D_v$ about -95 ‰ relative to VSMOW. The three curves show that as humidity decreases, $\delta D_v$ decreases. The cases of moist adiabatic ascent and remoistening of the air mass by drop evaporation contribute to the shape change from orange to green (after Noone, 2012). **(b)** Specific humidity profiles showing a decrease with height obtained from radiosonde data for the 29 selected days for BCIM runs (Run-2 and Run-3). The black bold line indicates the mean profile.

**S8 Vapour isotope profiles from AIRS and those adopted from TES**

Apart from the Tropospheric Emission Spectrometer (TES), vapour $\delta D_v$ data can be obtained from two other sources: the Atmospheric Infrared Sounder (AIRS) and the Infrared Atmospheric Sounding Interferometer (IASI).

We discuss this issue because it is possible that the predicted rain isotope ratios were greatly affected by our choice of TES satellite data. To explore this point, the following investigations were carried out.

Unfortunately, the IASI dataset was not available for the study period (June-September 2019). The AIRS dataset for that period was extracted over a 1° x 1° grid centered around our study location. The area-averaged $\delta D_v$ profiles for the selected 29 days, as obtained from the AIRS dataset, are shown in Fig. S10a and compared with the corresponding TES-derived profiles. It is seen that the AIRS values are significantly depleted at the surface compared to our measured values (Fig. S10a). We understand that this discrepancy stems from the lower accuracy of the AIRS satellite data in the near-surface or boundary layer. To circumvent this, we extrapolated the AIRS surface value linearly to match our measured surface values (Fig. S10b). Because AIRS data do not provide $^{18}O_v$ values, we estimated the $^{18}O_v$ values from the $\delta D_v$ values obtained from AIRS and the $d_v$ profiles used in Run-2. Afterwards, we ran the BCIM using these modified AIRS vapour isotope profiles to obtain the simulated rain isotope values. Next, we compared the observed and model $\delta D_r$ and $\delta^{18}O_r$ values (Fig. S10c, d). As evident from these figures, the model $\delta D_r$ and $\delta^{18}O_r$ values based on AIRS are far away from the 1:1 line. The deviations are much more compared with those calculated from TES profiles. This clearly demonstrates that using the AIRS profiles, we do not get good agreement, and in fact, there is more disagreement with the measured values compared to TES.

Next, we investigated the origin of deficiency in the AIRS data. The AIRS (Atmospheric Infrared Sounder) satellite data is less accurate at lower altitudes, specifically within the planetary boundary layer and near the surface. This is primarily due to challenges with infrared penetration through clouds, high humidity, and surface emissivity in the lower troposphere (Diao et al., 2013). Satellite retrievals of water vapour isotopes from the Tropospheric Emission Spectrometer (TES) provide direct measurements of HDO and $H_2O$ using the benefit of its high spectral resolution (Herman et al., 2014; Schneider et al., 2012). In contrast, isotope retrievals from the Atmospheric Infrared Sounder (AIRS) are derived using adapted TES retrieval algorithms and exhibit higher uncertainties and reduced sensitivity, particularly in the lower troposphere (Worden et al., 2019). Although AIRS-based $\delta D_v$ estimates are broadly consistent with TES, they are characterized by larger errors (~30‰ compared to ~15‰ for TES) and lower vertical sensitivity (Worden et al., 2019; Herman et al., 2020). In addition, we find that the near-surface AIRS values deviate systematically from the measured surface values (by about 50‰ in $\delta D_v$) because AIRS calculates atmospheric profiles while accounting for Earth's surface thermal radiation. Surface emissivity (how efficiently the surface emits infrared radiation) varies widely across land, making it difficult to accurately retrieve temperature and humidity in the first kilometer of the atmosphere. While AIRS is a powerful instrument for atmospheric sounding, these factors degrade its performance in the atmospheric boundary layer compared to the upper troposphere.

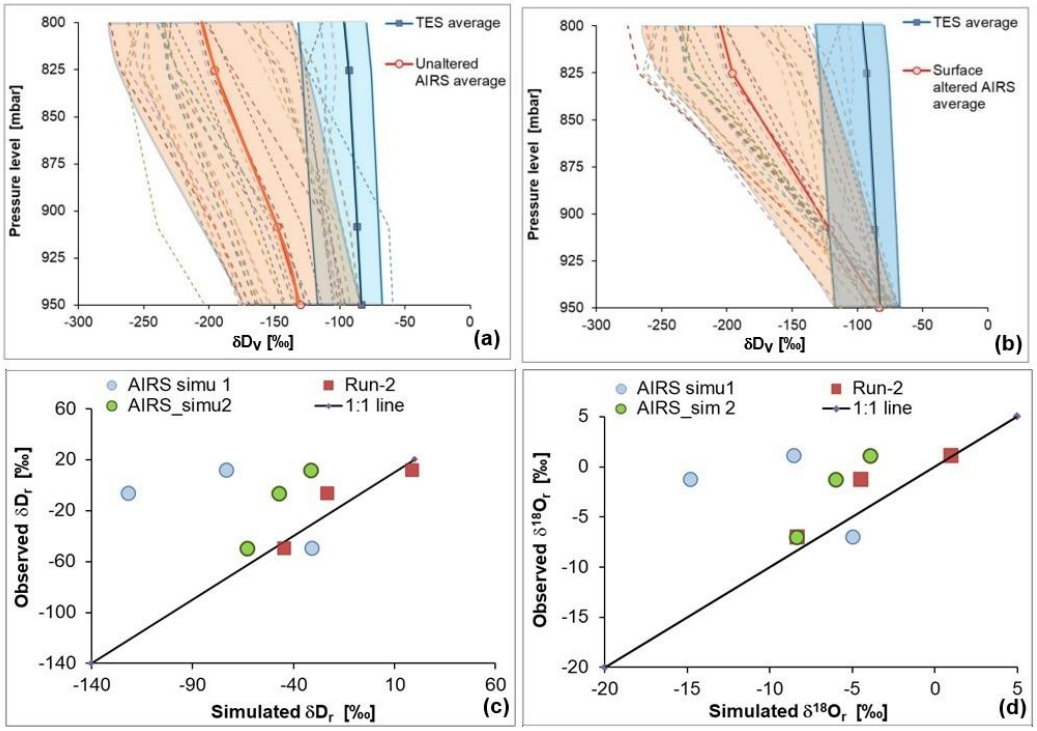


**Figure S10. (a)** Vertical variation of vapor $\delta D_v$ values as obtained from the AIRS dataset (orange envelope) and the $\delta D_v$ profiles constructed from TES values used for Run-2 (blue envelope). **(b)** Same as (a) but with surface values from the AIRS dataset, normalized to our surface observation. **(c)** Scatter plot showing model (Run-2) and observed $\delta D_r$ values using TES $\delta D_v$ profiles (red filled squares) and AIRS $\delta D_v$ profiles with (green filled circles) and without surface normalization (blue filled circle). The run was performed for three specific days- one with maximum observed $\delta D_r$ values, one with minimum and one with the closest to the mean $\delta D_r$ values. **(d)** Same as (c), but for $\delta^{18}O_r$ values.

### S9 Statistical Criteria to evaluate the performance of BCIM runs

Surprisingly, the outputs of Run-1 and Run-2 agree with each other reasonably well (see Fig. S11) for all three isotopic

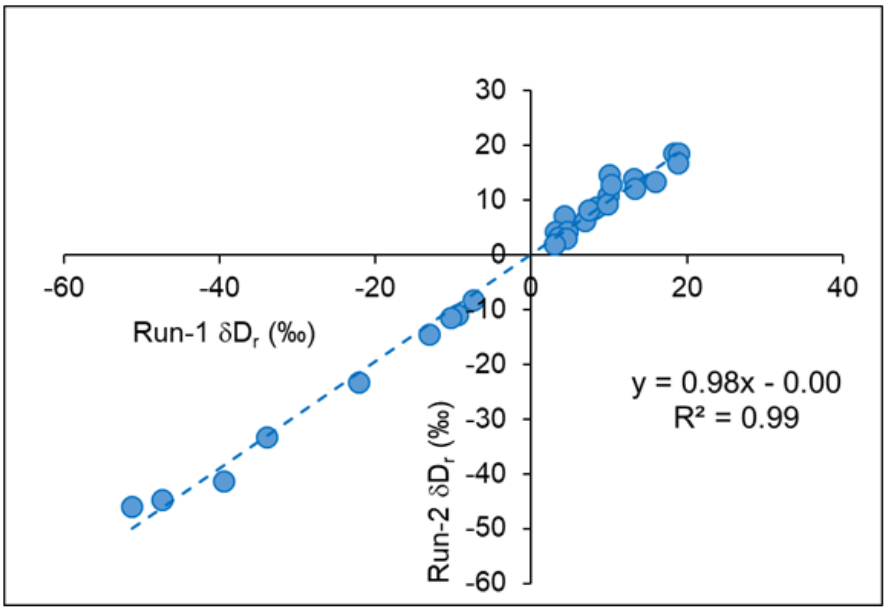


**Figure S11.** Rain $\delta D_r$ values of Run-2 plotted against those of Run-1 show good agreement among them despite differing RH profiles.

parameters, but they do not agree well with the observed values. The differences are on the order of ±10 ‰ in $\delta D_r$.

To check the performance of all three runs, a two-tailed Student's t-test with observed and modeled $\delta^{18}O_r$, $\delta D_r$, and d-excess, ($d_r$) values is carried out after each run. The null hypothesis states that the observed and model population means are not significantly different at a significance level of p = 0.05. The p-values for all three runs are given in Table S3. We look for that run in which p is greater than the significance level for all three isotope ratios.

**Table S3.** The p-values of Student t-tests performed with observed and model rain isotope ratios ($\delta^{18}O_r$, $\delta D_r$ and $d_r$)

| Rain isotope values | Run-1 | Run-2 | Run-3 |
|---|---|---|---|
| $\delta^{18}O_r$ | 0.54 | 0.34 | 0.86 |
| $\delta D_r$ | 0.45 | 0.44 | 0.84 |
| $d_r$ | 0.00 | 0.00 | 0.95 |

A reasonable agreement between observed and model values is considered to exist when the null hypothesis is valid for all three parameters ($\delta^{18}O_r$, $\delta D_r$, and $d_r$). The p-values in Run-1 and Run-2 do not qualify for this (p is less than 0.05 for d-excess), but Run-3 meets this criterion (p values for all three are greater than 0.05). Therefore, we consider that the model means are not significantly different from the observed means for Run-3 (as designed by tuning).

**S10 Uncertainties in rain δD(δD$_r$) and d-excess (d$_r$)using Run-3 results**

Using the Run-3 model output values, we obtained a multi-parameter regression equation for $\delta D_r$ as a function of the four variables (vapour isotope, relative humidity, temperature and drop diameter) $\delta D_v$, RH, T and D as below:

$$\delta D_r = 87.88 + 1.137* \delta D_v - 0.257* RH + 1.052* T - 3.785* D \qquad (1)$$

A similar multiple regression for $d_r$ yields the equation.

$$d_r = -10.5557 + 0.60164* d_v + 0.169599*RH - 0.31632*T + 2.2921*D \qquad (2)$$

Using the standard quadratic formula for error (Farrance and Frenkel, 2012), when the dependent variable $\delta D_r$ is a function of $\delta D_v$, RH, T, and diameter D, the error $\sigma(\delta D_r)$ is given by:

$$\sigma(\delta D_r)^2 = (\delta D_r/\delta D_v)^2*\sigma(\delta D_v)^2 + (\delta D_r/RH)^2*\sigma(RH)^2 + (\delta D_r/T)^2*\sigma(T)^2 + (\delta D_r/D)^2*\sigma(D)^2 \qquad (3)$$

Where σ denotes the uncertainties in $\delta D_v$, RH, T and D, and the quantities in brackets express the partial derivative of $\delta D_r$ with respect to the variable. The regression coefficients were used as the partial derivatives. The vapour isotope $\delta D_v$ has an error of 2 ‰. The absolute uncertainties associated with RH and T in radiosonde observations are 8% and 0.3 °C (Sapucci et al., 2005), but these vary from day to day. We can take the absolute difference as the daily scale uncertainty. The error for each day is then taken as the absolute difference divided by √2 (to get the standard error of the mean of two observations).

To obtain the drop diameter error, we note that the mean and standard deviation of the drop diameters (calculated from the Marshall-Palmer relation using the rain rates) based on all 29 rain samples are 1.00 mm and 0.3 mm, respectively, i.e., the standard deviation is about 30% of the mean diameter. We could have taken 30 % of the mean diameter as the common average uncertainty. However, Tokay et al. (2001) quote an uncertainty estimate for the drop diameter, derived from the Marshall-Palmer distribution, of about 20%, which we adopt. Pune drop diameter varies from 0.61 mm to 1.80 mm over the 29 days. Taking the error in each day's diameter as 20 % of that day's value, the individual error varies from 0.12 mm to 0.36 mm. Adding these three errors using the above quadratic formula, we obtain the error in the evaporation fraction for 29 days, which varies from 7.4 % to 13.8 % (with corresponding EF values varying from 4 % to 61%). The average EF for 29 days is ±8.9 %, which is taken as the overall error (common for all days) in the evaporation estimate. With these inputs, the mean uncertainty in the rain isotope value $\delta D_r$ is 3.5 ‰. Using a similar exercise for the $d_r$, we obtain a mean uncertainty of 1.7 ‰.

**S11 Sensitivity of model rain composition using Run-3 results**

We conducted a sensitivity analysis of the model rain composition using the Run-3 case to examine the effects of variations in $\delta D_v$, RH, T, and D. We ran multiple simulations, changing one parameter at a time while keeping the others constant, and compared the $\delta D_r$ values with the reference run. The Fig. S12 shows that the vapour isotope value is the most important factor in controlling the model rain isotope ratios. For +10 % change over the reference value of the parameters, the changes in the $\delta D_r$ values (in ‰) are: +7.6 (for $\delta D_v$), -4.1 (for RH), +2.6 (for T), and -0.4 (for D). Interestingly, the temperature effect is the opposite to that expected from evaporation: lower temperatures yield lower isotope ratios. This is because the higher enrichment from fractionation at lower

temperatures in the drop-formation zone offsets the lower evaporative enrichment at lower temperatures on the way down.

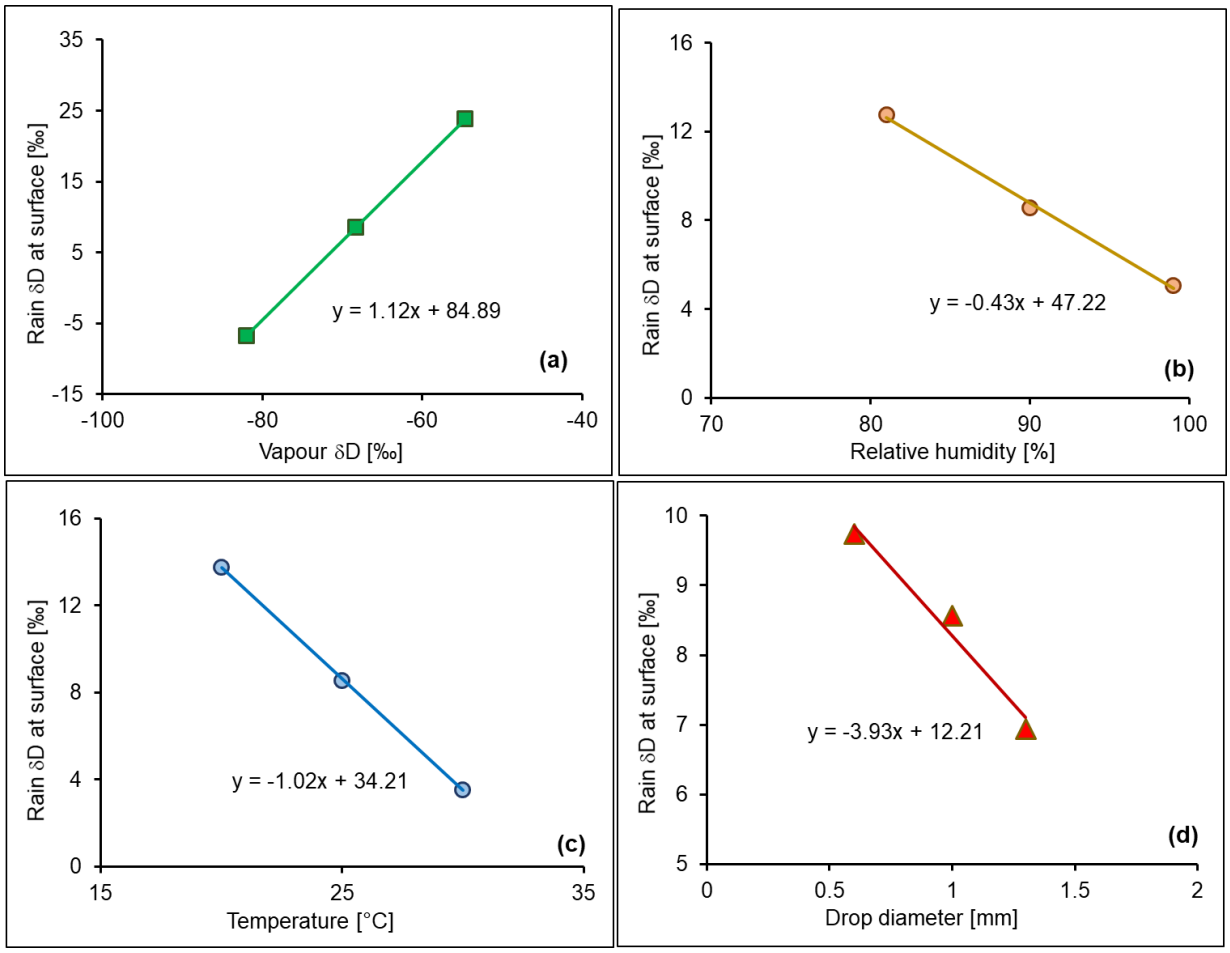


**Figure S12**. The sensitivity of model $\delta D_r$ values on the values of various parameters using the Run-3 case. Four parameters are considered: **(a)** $\delta D_v$, **(b)** Relative humidity, **(c)** Temperature, and **(d)** Drop diameter. A change of ±20 % (for $\delta D_v$), ±10 % (for RH) and ±20 % (for T), ±30 % (for D) was imposed to see the impact of the change in model rain values. The vapour $\delta D_v$ value has the maximum impact on the model rain isotope value.

A sensitivity analysis can also be conducted to evaluate the impact of the formation height while keeping all other parameters constant. We increase the formation height by 1 km (from 1.5 km to 2.5 km) and run the BCIM. To form the drop at a higher altitude, we need to extend the RH profile so that the 100% RH level is maintained to the new height. Similarly, the vapour isotope profiles and temperature profiles are also extended. Interestingly, the simulated values of the rain isotope ratios did not change significantly. Similarly, the raindrop evaporation fraction also did not change significantly.

**S12 Relationship of vapour isotopes with meteorological parameters**

The relationships between local meteorological parameters (surface relative humidity, air temperature obtained from the IMD observatory at Pune) and specific humidity (derived from the above parameters) and d-excess of vapour samples measured near the surface are plotted in Fig. S13. Our aim is to investigate whether local meteorological conditions influence isotopes.

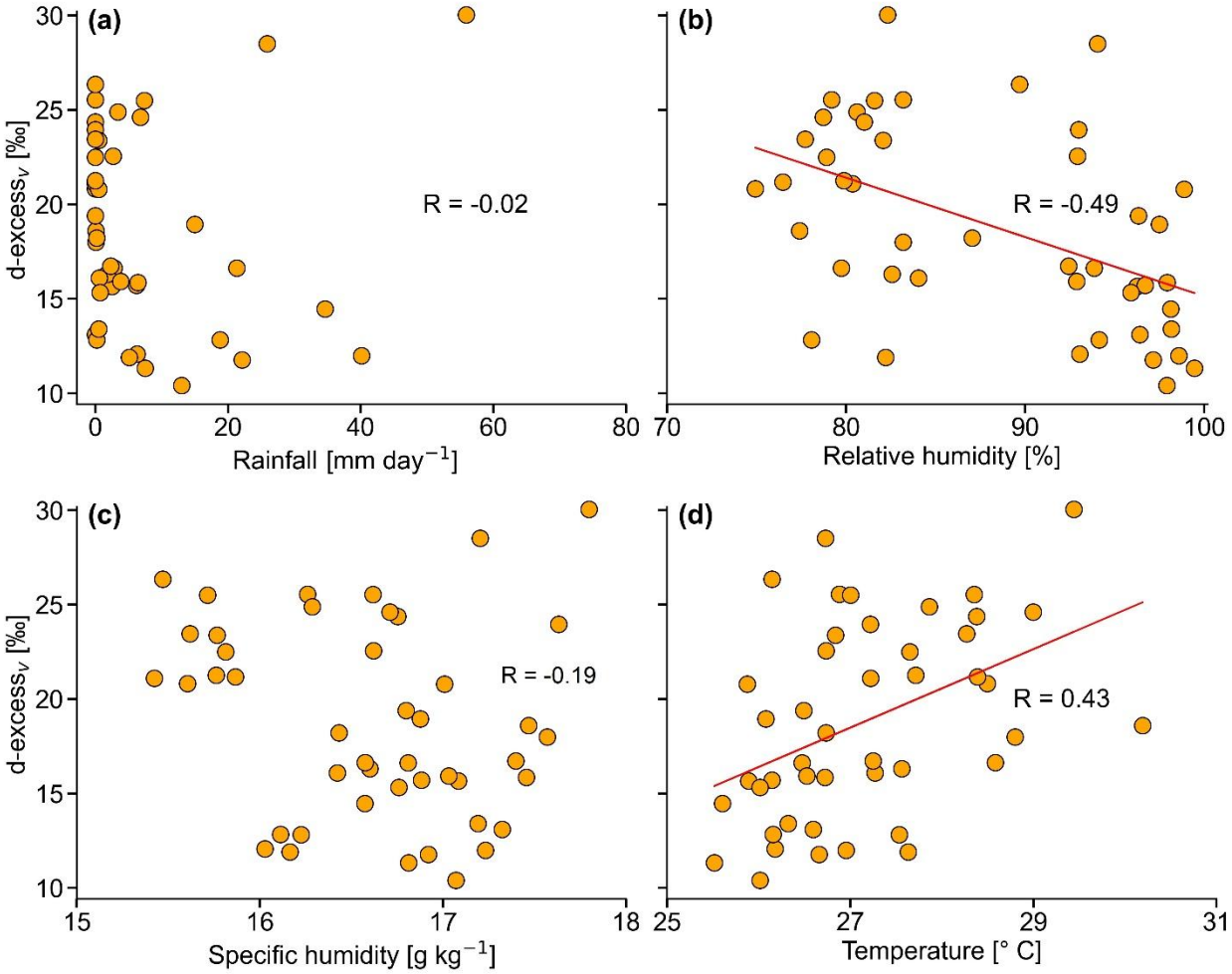


**Figure S13.** Water vapour d-excess values ($d_v$) measured at Pune plotted against **(a)** Rainfall, **(b)** Relative humidity, **(c)** Specific humidity and **(d)** Temperature for the corresponding days.

**S13 Slope of linear fit in Δδ–Δd diagram using the Bootstrap Method**

We have defined two quantities in the Main text for exploring the rain vapour exchange, as below:

Δδ = δD (rain eq. vapour) - δD (surface vapour) and similarly for d-excess, and

Δd = d-excess (rain eq. vapour) - d-excess (surface vapour)

These quantities evaluate the isotopic departure of rain samples from surface vapour in terms of rain-equilibrated vapour (see main text). It is important to understand the factors responsible for the slope value in the Δδ–Δd plot.

The slope is essentially due to the following differential effects in evaporative fractionation. Evaporation decreases $d_r$ but increases its $\delta D_r$. However, the magnitudes of these changes, negative for d-excess and positive for δD, are not the same. Fractionation values (involving equilibrium and kinetic factors) show that the change in δD is larger than that in d-excess (about 30% of the δD change, considering the absolute values for the changes). This is because in evaporation, the kinetic effect operates in addition to the equilibrium effects, and that has more influence on δD compared to $\delta^{18}O$. If the kinetic fractionation is higher than normal (due to higher temperature and lower RH), the deviation from the equilibrium fractionation line will be greater, and the slope (in Δδ–Δd plot) will be higher. In the frontal systems of Switzerland, the temperature was about 12° C, and RH was about 80% (from Graf et al., 2019), compared to Pune, where the temperature was between 25° C to 30° C and RH was about 85 %. Since we know that temperature plays an important role (nearly as much as RH for evaporation; see coefficients of the normalized multiple regression equation for evaporation fraction, 0.370 against -0.329 in the multiple regression equation: Evaporation Fraction = -0.329* RH +0.370* Temperature -0.665* Diameter), for the larger values of Pune temperatures we expect more evaporation, which leads to the higher slope value of -0.45 for Pune compared to -0.30 for Zurich. For calculation of the slope for Pune we use the Bootstrap method (as shown in Fig. S14), yielding a mean value of -0.45.

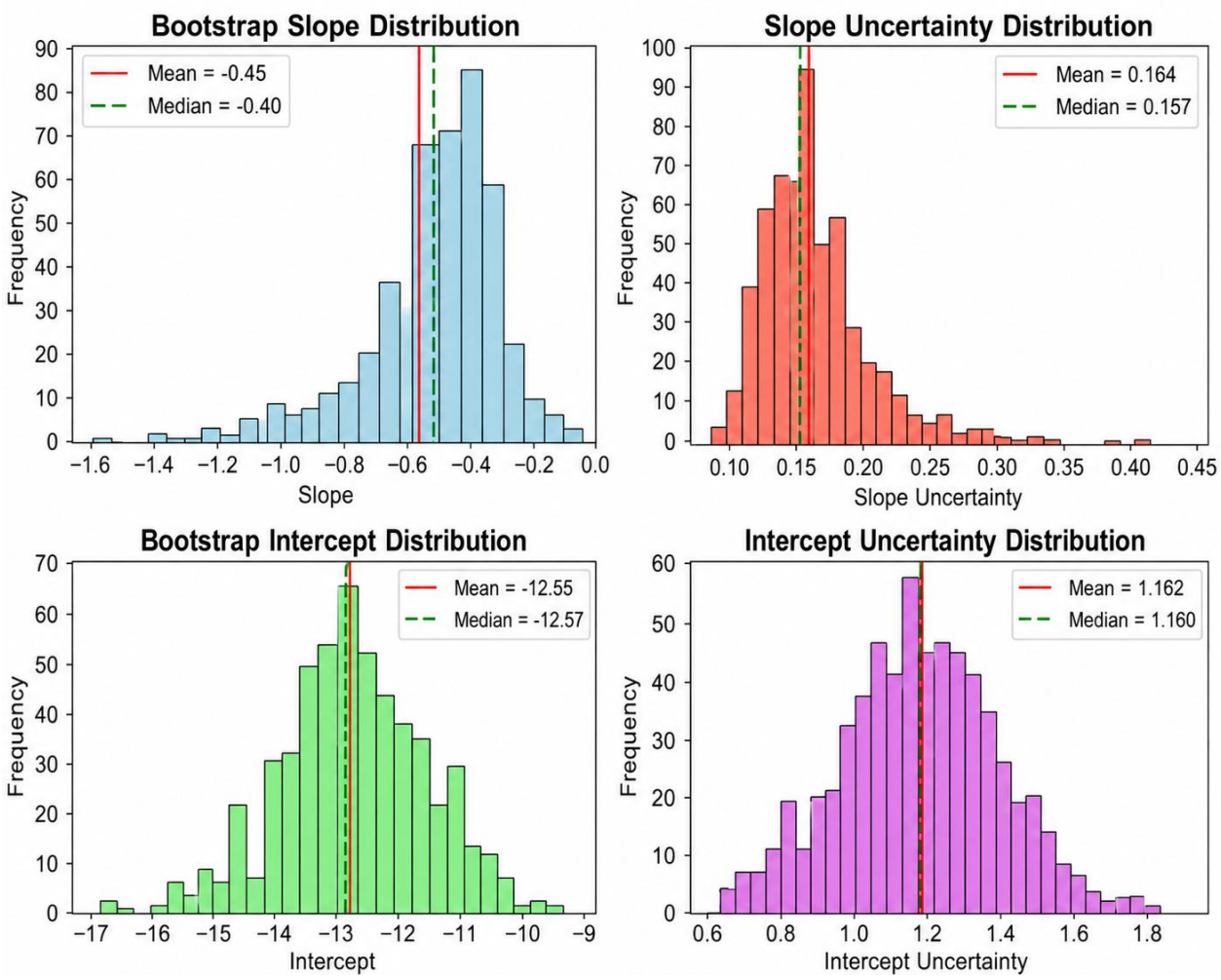

**Figure S14**. Distributions of the slope and intercepts for Pune (in Δδ–Δd plot) along with their associated uncertainties calculated by the Bootstrap method. The bootstrap-estimated mean slope is -0.45.

Our data, in a simple Excel analysis, yield a slope of -0.30. But we believe that a bootstrap analysis provides a better slope value because, unlike excel, it is not sensitive to the few highly deviant points. Since the deviant points are given appropriate status in the Bootstrap analysis (Davison and Hinkley, 1997) we obtain a more realistic slope value. The Bootstrap analysis was performed by taking 20 random samples of size 29 from the full set of 29 samples each time, fitting the points, and repeating this 1000 times. The distribution of the slope values along with the mean, median, and standard deviation is given in these plots. Additionally, the Bootstrap method provides a realistic measure of uncertainty distribution.

**S14 Errors introduced into the BCIM simulation by using average radiosonde profiles**

On operating days, the radiosondes are usually launched at 00 Z and 12 Z in Pune. The radiosonde data (the average of these two daily observations) for Pune are expected to be reasonable for use in the model if we can show that the difference between the two consecutive measurements is small. The difference between RH (ΔRH) and temperature (ΔT) measured at 12 Z and 00 Z is plotted against height in Fig. S15 for the 29 days that are considered in the BCIM runs. The figure shows that the ΔRH values are within ±10% on most days (~80% of the total sampling days), and the ΔT values are within 2 °C. As a measure of uncertainty we can take the average of the absolute differences. This is acceptable because those two parameters over western India do not vary much during the Indian Summer Monsoon (Pathak et al, 2014). However, we need to check how big these differences are in the context of their use in the model. We have shown through sensitivity analyses and two multiple regression analyses (see Main text) that the effects of daily-scale variation in RH and T on model rain isotope values and the evaporation fraction are not significant.

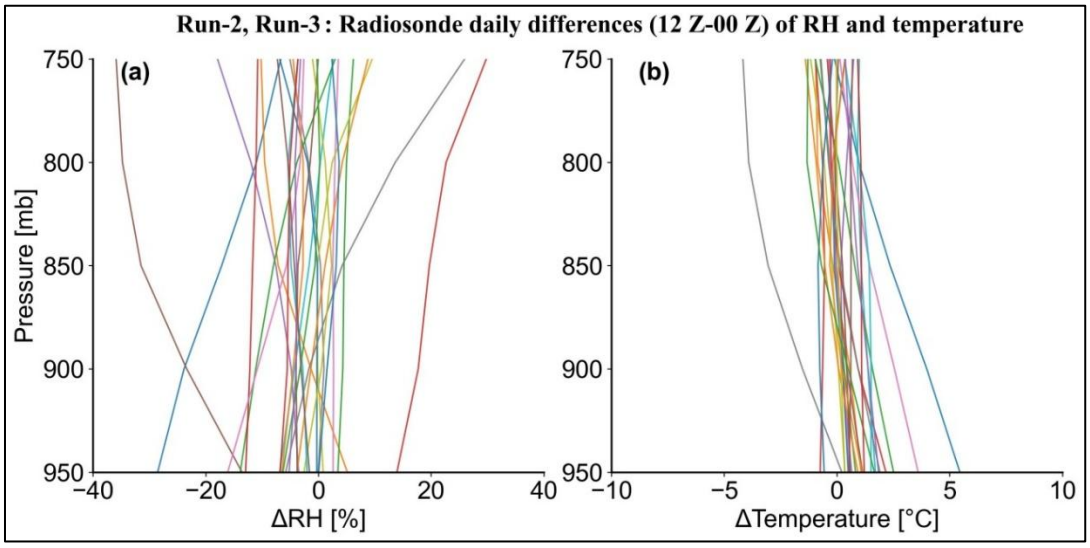

**Figure S15.** The **(a)** RH and **(b)** temperature differences (ΔRH, in % and ΔT, in °C) between two radiosonde measurements (12 Z data minus 00 Z data) of each day versus altitude (in mb). The profiles of these differences for the 29 days considered show that, for most of the days, the differences are not large and the mean value of each day can be used without compromising the quality of model simulations.

**References**


Bony, S., and Emanuel, K. A.: A parameterization of the cloudiness associated with cumulus convection; Evaluation using TOGA COARE data, J. Atmos. Sci., 58, 3158–3183, https://doi.org/10.1175/1520-0469(2001)058<3158:APOTCA>2.0.CO;2, 2001.

Craven, J. P., Jewell, R. E., and Brooks, H. E.: Comparison between observed convective cloud-base heights and lifting condensation level for two different lifted parcels, Weather Forecast., 17(4), 885-890, https://doi.org/10.1175/1520-0434(2002)017<0885:CBOCCB>2.0.CO;2,2002.

Draxler, R. R., and Hess, G.: Description of the HYSPLIT4 modeling system, 1997.

Davison, A. C., and Hinkley, D. V.: Bootstrap Methods and Their Application, Cambridge University Press https://doi.org/10.1017/CBO9780511802843, ISBN:9780511802843, 1997.

Diao, M., Jumbam, L., Sheffield, J., Wood, E. F., and Zondlo, M. A.: Validation of AIRS/AMSU-A water vapor and temperature data with in situ aircraft observations from the surface to UT/LS from 87°N–67°S, J. Geophys. Res. Atmos., 118, 6816–6836, https://doi.org/10.1002/jgrd.50483, 2013.

Emanuel, K. A.: A scheme for representing cumulus convection in large-scale models, J. Atmos. Sci., 48, 2313–2329, https://doi.org/10.1175/1520-0469(1991)048<2313:ASFRCC>2.0.CO;2, 1991.

Ernest Raj, P., Devara, P. C. S., Pandithurai, G., and Sharma, S.: Cloud base height estimation based on Laser radar at Pune, Indian J. Radio Space Phys., 25, 74-78, 1996.

Farrance, I., and Frenkel, R.: Uncertainty of Measurement: A review of the rules for calculating uncertainty components through functional relationships, Clin. Biochem. Rev., 33(2), 49–75, 2012.

Graf, P., Wernli, H., Pfahl, S., and Sodemann, H.: A new interpretative framework for below-cloud effects on stable water isotopes in vapour and rain, Atmos. Chem. Phys., 19, 747–765, https://doi.org/10.5194/acp-19-747-2019, 2019.

Grandpeix, J. Y., Phillips, V., and Tailleux, R: Improved mixing representation in Emanuel's convection scheme, Q. J. R. Meteorol. Soc., 130, 3207–3222, https://doi.org/10.1256/qj.03.144, 2004.

Hourdin, F., Musat, I., Bony, S. et al.: The LMDZ4 general circulation model: climate performance and sensitivity to parametrized physics with emphasis on tropical convection, Clim. Dyn, 27, 787–813, https://doi.org/10.1007/s00382-006-0158-0, 2006.

Kanamitsu, M.: Description of the NMC Global Data Assimilation and Forecast System, Weather Forecast., 4, 335–342, https://doi.org/10.1175/1520-0434(1989)004<0335:DOTNGD>2.0.CO;2, 1989.

Noone, D.: Pairing measurements of the water vapor isotope ratio with humidity to deduce atmospheric moistening and dehydration in the Tropical Mid-troposphere, J. Climate, 25(13), 4476-4494, https://doi.org/10.1175/JCLI-D-11-00582.1, 2012.

Pathak, A., Ghosh, S., and Kumar, P.: Precipitation recycling in the Indian subcontinent during summer monsoon, J. Hydrometeorol., 15, 2050–2066, https://doi.org/10.1175/JHM-D-13-0172.1, 2014.

Rajaveni, S. P., Nimya, S. S., Sengupta, S., Datye, A., and Sarma, D.: Three years of stable water isotope data of daily rain samples collected from three geomorphic regions of India, Sci. Data, 11, 1445, https://doi.org/10.1038/s41597-024-04308-7, 2024.

Sapucci, L. F., Machado, L. A. T., Da Silveira, R. B., Fisch, G., and Monico, J. F. G.:Analysis of relative humidity sensors at the WMO Radiosonde Intercomparison Experiment in Brazil, J. Atmos. Oceanic Technol., 22, 664-678, 2005.

Song, H., Kim, S., Lee, H., and Kim. K.: Climatology of tropospheric relative humidity over the Korean Peninsula from Radiosonde and ECMWF Reanalysis, Atmosphere, 11(7), 704, https://doi.org/10.3390/atmos11070704, 2020.

Tokay, A., Kruger, A., and Krajewski, W. F.: Comparison of drop size distribution measurements by impact and optical disdrometers, J. Appl. Meteor. Climatol., 40(11), 2083–2097, https://doi.org/10.1175/1520-0450(2001)040<2083:CODSDM>2.0.CO;2, 2001.

Van Leer, B.: Towards the ultimate conservative difference scheme: IV. A new approach to numerical convection, J. Comput. Phys., 23, 276–299, https://doi.org/10.1016/0021-9991(77)90095-X, 1977.